Ultrasonic Devulcanization of Rubber Vulcanizates. II. Simulation and Experiment

A. I. ISAYEV,* S. P. YUSHANOV, and J. CHEN

Institute of Polymer Engineering, University of Akron, Akron, Ohio 44325-0301

SYNOPSIS

The simulation results based on the devulcanization model presented in Part I of this study are described for devulcanization of SBR vulcanizates. The vulcanizates are conveyed by a single-screw extruder to a thin gap between a stationary die and a vibrating horn. Gapwise velocity, temperature, and shear-rate distributions along the die length are calculated. Predictions of the model for changes of various structural characteristics including gel fraction, fraction of various broken bonds, rate of their breakup, and void formation along die length are given. Devulcanization energy consumption and energy dissipated by ultrasonic waves are calculated. Comparison of these energies indicates that the devulcanization energy represents only a small fraction of the dissipated energy. The predicted results for gel fraction, crosslink density, die characteristics, and "mixing cup" temperature are compared with the experimental data. These predicted results are found to be only in qualitative agreement with experimental observations. The theoretical and experimental results indicate that the rubber is partially devulcanized and the devulcanization process is accompanied by some degradation of the macromolecular chains. © 1996 John Wiley & Sons, Inc.

INTRODUCTION

In Part I of this study,[1] a mathematical model of the continuous devulcanization process was proposed. The proposed model was based upon a mechanism of rubber network breakup caused by cavitation which is created by high-intensity ultrasonic waves in the presence of pressure and heat on rubber vulcanizates. The analysis of model parameters was carried out and a simulation algorithm described. In Ref. 2, various devulcanization experiments were carried out with model styrene–butadiene rubber (SBR). Structural characteristics of devulcanized SBR, such as gel fraction, crosslink density, and molecular weight of the sol fraction were measured. It is of interest to determine how the theory proposed in Ref. 1 is able to describe experimental observations. Therefore, the main purpose of the present article was to carry out the detailed simulation of the devulcanization process for various processing conditions and to compare predicted results with previously reported[2] experimental data.

EXPERIMENTAL

A solution-polymerized styrene–butadiene rubber Duradene 706 manufactured by the Firestone Co. was used in the present experiments. It contains 23.5% bound styrene, 76.5% butadiene, and a nonstaining antioxidant stabilizer system. The weight-average molecular weight and polydispersity index of the SBR measured by gel permeation chromatography (GPC) were found to be $2.86 \cdot 10^5$ (g/mol) and 2.3, respectively. A recipe of the prepared compound includes 1.5 and 1.0 part, respectively, of sulfur and santocure, per 100 parts of SBR. The rubber and curing ingredients are mixed using a two-roll mill (Albert) by passing the material through the nip of the rolls approximately 30 times. The prepared compounds are vulcanized in a compression-molding press at 171°C for 30 min. The vulcanizates are chopped and charged into an ultrasonic reactor. The reactor consists of a 1 in. Killion laboratory plastic extruder with a length to diameter ratio $L/$

* To whom correspondence should be addressed.

Journal of Applied Polymer Science, Vol. 59, 815–824 (1996)
 CCC 0021-8995/96/050815-10

D = 24 and an ultrasonic crosshead die attachment (see Fig. 1). A 900 W ultrasonic power supply, a converter, and a booster are used to provide the longitudinal vibrations of the horn with a frequency of 20 kHz. The horn diameter is 12.7 mm, the diameter of the die opening is 6.35 mm, and the gap between the flat face of the horn and the chamber bottom is 0.5 mm. The temperature of the extruder barrel, T_b, is fixed at 120°C. The amplitude of the horn oscillations, A, and the screw rotation speed are varied.

The devulcanized samples are obtained at various processing conditions. The flow rate, pressure at the die entry, and the material temperature are measured. In the present setup, it is difficult to control the melt temperature in the die due to significant heat generation by the ultrasonics. Thus, various die temperatures are achieved for each processing condition depending on the amplitude and the residence time of the material in the die. The die and horn are not cooled in these experiments.

A Monsanto processibility tester is utilized for the viscosity measurements of virgin and devulcanized SBR. The viscosity is measured in the shear rate range of 1–1000 s^{-1} at temperatures of 70, 100, and 130°C. A Monsanto tensiometer (Model 10) is used to obtain the stress–strain characteristics of cured virgin compound. The dumbbell samples for tensile testing are punched from the cured rubber sheets using the ASTM D412, type C, die. The measurements are carried out at room temperature at an elongation rate of 25 mm/min.

The gel fraction of the devulcanized SBR is measured by a BFGoodrich device according to ASTM D3616 using benzene as the solvent. The crosslink density of the vulcanized and devulcanized rubbers is measured using a swelling technique proposed by Flory.[3] Benzene is used in the swelling experiments.

The GPC technique is used to measure the molecular weight and the polydispersity index of the soluble component in the devulcanized SBR. Polystyrene samples with narrow molecular weight distribution are used for the calibration.

Evidence of Cavitation

The evidence most directly linked to cavitation in the devulcanization process has come from specially designed static experiments. In these experiments, a power supply of 900 W along with converter, booster, and horn is used to generate ultrasonic waves of frequency of 20 kHz and amplitudes up to 40 μm. An SBR rubber sheet was placed between horn and fixed plate at temperature 150°C. It was found that at an ultrasonic amplitudes above 5 μm some cavities of ~ 1 mm were created in the SBR sheet after ultrasonic treatment. In addition, the originally transparent SBR sheet became milky, indicating the presence of tiny microbubbles in the treated samples.

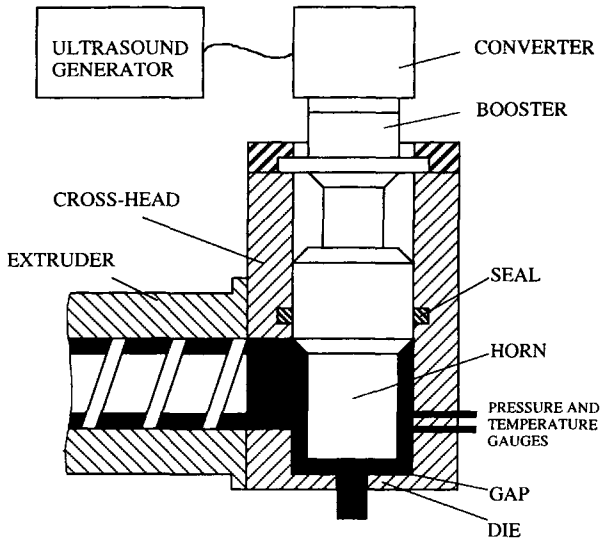

Figure 1 Schematic of the devulcanization reactor.

Other indirect evidence of cavitation comes from observation of the horn surface. After prolonged use, surface damages were observed at the die and horn surfaces. This type of damage is similar to the damage caused by high-speed liquid jets impacting solid surfaces, producing tiny pits or crates on the solid surfaces.[4]

These experiments clearly show the existence of cavitation in rubber vulcanizates in ultrasonic field at certain conditions. The existence of cavities in polymer melt during ultrasonic treatment was also observed in earlier investigations.[5–7]

Rheology

To simulate the rubber flow process, one must specify the rheological properties of the material. A modified power-law model is employed to describe the flow behavior of devulcanized rubber obtained under various processing conditions:

$$\eta = Be^{\frac{b(\xi)}{RT}}\dot{\gamma}^{n-1} \tag{1}$$

As indicated in eq. (1), the parameters B and n along with a polynomial function $b(\xi) = b_0 + b_1\xi + b_2\xi^2$ specify viscosity η as a function of shear rate $\dot{\gamma}$, temperature T, and gel fraction ξ. The flow curves for each devulcanized rubber was obtained at various temperatures. The gel fraction of the devulcanized

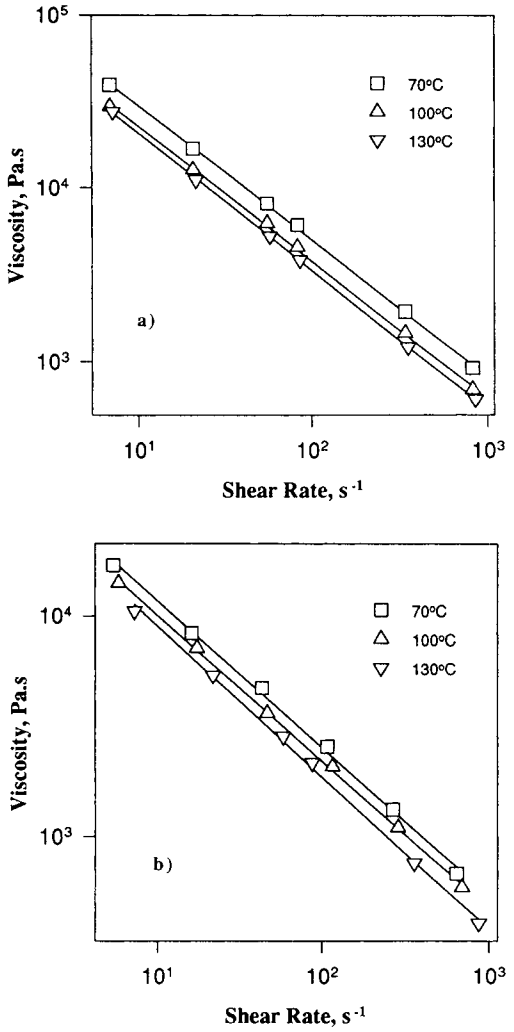

Figure 2 Flow curves of devulcanized SBR rubber at various temperatures and gel fractions: (a) $\xi = 0.761$; $A = 28$ μm; $Q = 0.39$ cm^3/s; (b) $\xi = 0.621$; $A = 31.5$ μm; $Q = 0.205$ cm^3/s.

rubber obtained in experiments varies from 0.761 to 0.621. Figure 2(a) and (b) show flow curves of the devulcanized samples having highest and lowest gel fractions, 0.761 and 0.621, respectively. Comparison of these figures indicates that the devulcanized rubber of the lower gel fraction exhibits lower viscosities. It is also seen that the flow curves indeed exhibit power-law behavior.

At a constant gel fraction and various temperatures, flow curves of the devulcanized rubber are found to superimpose to a flow curve at some reference temperature, T_r, by shifting along the shear rate axis. In the present case, the value of T_r of 70°C is chosen. By carrying out this procedure, the shift factor as a function of temperature is determined at a constant gel fraction. The shift factors as a function of gel fraction at various temperatures are shown in Figure 3. Then, the second shift that is performed is one in which the reduced flow curves at the reference temperature and various gel fractions are superimposed to a master curve corresponding to some reference gel fraction, ξ_r. The master curve for reduced viscosity vs. reduced shear rate is given in Figure 4. The value of $\xi_r = 0.761$ is chosen as reference gel fraction to obtain this master curve. Some scattering of the data is seen, especially in the region of high shear rates. This scattering is due to the use of a constant power-law index. In fact, some deviation of the power-law index n is found as gel fraction in devulcanized rubber is var-

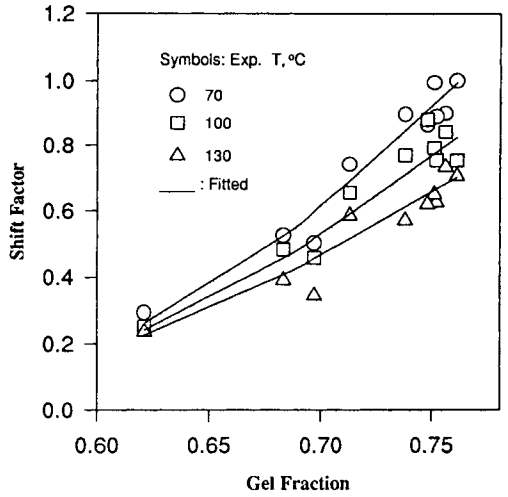

Figure 3 Fitted (curves) and experimental (symbols) shift factors vs. gel fraction at various temperatures.

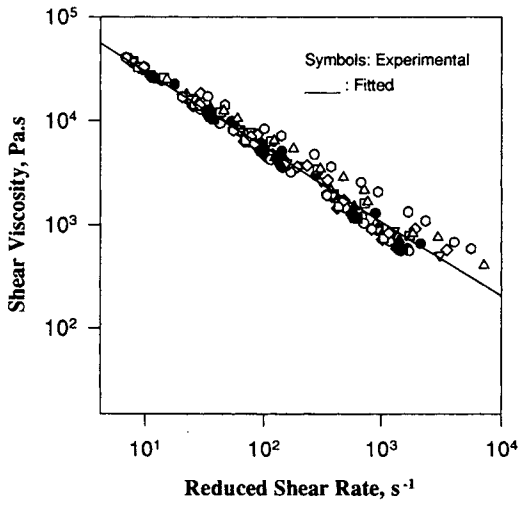

Figure 4 Fitted (curves) and experimental (symbols) master curve of viscosity vs. shear rate at $T_r = 70$°C and $\xi_r = 0.761$.

Table I Geometric Dimensions of the Die

Description	Symbol, Unit	Value
Horn radius	R_1, mm	6.35
Botton plate hole radius	R_2, mm	3.175
Gap clearance	$2h$, mm	0.5

ied.[2] Apparently, a modified Cross model[8] would be a better model for describing the viscosity function of devulcanized rubber. However, a power-law model used here adds a simplicity to the present treatment of the devulcanization process.

The parameters in eq. (1) are determined by curve fitting the data depicted in Figures 3 and 4 using the least-squares method. The values of these parameters are found to be $B = 1.5 \cdot 10^4 \text{Pas}^{2-n}$, $b(\xi) = 859 - 950\xi + 9162\xi^2$ (JK/mol) and $n = 0.28$. The fitted curves are shown by the solid lines in these figures.

SIMULATION RESULTS

All the input data utilized for the devulcanization process simulation are summarized in Tables I–III. The model parameters N_0, β, and R_0 were discussed in Part I of this study. The fitting parameter K has been chosen in such a way to fit the theoretical predictions of gel fraction with the experimental data. A finite-difference mesh of 20×20 has been adopted for this simulation.

Simulation is carried out for the various devulcanization conditions. The results presented in this section correspond to initial temperature of the material $T_0 = 418$ K, die wall temperature $T_w = 444$ K, ultrasound frequency $f = 20$ kHz, ultrasonic amplitude $A = 31.5$ μm, and flow rate varying from $Q = 0.1$ to 0.4 cm^3/s.

Figure 5 shows the gapwise distribution of velocity at various cross sections in the die. The velocity increases as the rubber moves from the die entrance toward the die exit. This increase in the velocity is due to a decrease in cross-sectional area of the disk die. The shape of the velocity profile also changes. At the die entrance, the velocity profile is flatter than at the die exit. The latter is caused by the temperature profile variation as rubber is heated up due to the ultrasonic dissipation, as indicated in Figure 6. In particular, rubber enters the die under uniform temperature, T_0. It is continuously heated up as the distances away from the wall increase and as the rubber moves toward the die exit. This increase in temperature leads to a decrease in the viscosity in the core region. In turn, the viscosity reduction in the core affects the velocity and shear rate profiles. Distributions of shear rate at various die cross sections are presented in Figure 7. The shear rate has a maximum value at the die wall where the velocity has maximal gradient, and it is equal to zero at the die middle plane $z = 0$ due to flow symmetry with respect to this plane. Due to the uniform temperature of the material at the die entrance, the slope of shear rate profile at this location is seen to continuously increase toward the die wall as expected for the case of fully developed flow. However, it is interesting to note that the shear rate at the wall of the die entrance is higher than that in the cross

Table II Physicomechanical Properties

Description	Symbol, Unit	Value	Source
Specific heat	c_p, J/(kg K)	1884	Ref. 9
Thermal conductivity	k_{th}, J/(m s K)	0.22	Ref. 9
Density	ρ_0, kg/m^3	930	Ref. 9
Surface tension	σ, N/m	0.036	Ref. 9
Ratio of specific heats of gas	γ	1.4	Ref. 10
C—C bond energy	E_c, kJ/mol	352	Ref. 11
C—S—C bond energy	E_s, kJ/mol	285	Ref. 11
C—S—S—C bond energy	E_{ss}, kJ/mol	268	Ref. 11
Initial crosslink density	ν_0, kmol/m^{-3}	$6.8 \cdot 10^{-2}$	Experiment
Initial gel fraction	ζ_0	0.958	Experiment
Loss Young's modulus	E'', MPa	1	Ref. 12
Stored-energy constant[a]	W_1, MPa	0.12	Experiment
Stored-energy constant[a]	W_2, MPa	0.085	Experiment

[a] Stored-energy potential is defined as $W = W_1(I_1 - 3) + W_2 \ln\left(\frac{1}{3} I_2\right)$, with I_1, I_2 being strain invariants.

Table III Model Parameters

Parameter	Symbol, Unit	Value	Description
Void initial radius	R_0, μm	25	
Void formation parameter[a]	β, MPa^{-1}	10	Ref. 1
Void formation parameter[a]	N_0, m^{-3}	$4.7 \cdot 10^3$	Ref. 1
Fitting parameter	K, m/s	$3.4 \cdot 10^{-5}$	Eq. (4), Ref. 1

[a] No. voids formed is adopted as [13] $N_b = N_0 \exp(\beta P_h)$, with P_h being negative driving pressure.

section next to the entrance; even the cross-sectional area at this location is decreased. This is due to a fast temperature increase in the core caused by ultrasonic heat dissipation as indicated by Figure 6.

Figure 8 shows variations in the pressure along the die length for various flow rates. A flow rate decrease results in pressure reduction. With increasing distance from the die entrance, the pressure decreases monotonically, approaching to atmospheric pressure at the die exit. The pressure gradient along the die length is not constant. The pressure gradient is highest at the die entrance and decreases monotonically as the rubber moves toward the die exit. The decreasing of the pressure gradient is caused by the viscosity reduction due to devulcanization process and temperature increase due to ultrasonic energy dissipation as the rubber passes through the die gap. This conclusion can be made based on Figure 9, which depicts gel fraction variation as a function of distance from the entrance. In particular, the gel fraction decreases monotonically. However, the rate of the gel fraction reduction shows more complicated behavior depending on the flow rate. At a low flow rate, the rate of gel fraction reduction is highest at the die entrance [curve 1 on Fig. 9(a)], while at elevated values of the flow rate, the region of highest gel fraction rate reduction is located in the vicinity of the die exit [curves 3 and 4 on Fig. 9(a)]. It is interesting to determine if the observed behavior of gel fraction is related to residence time of rubber in the die. In this regard, Figure 9(b) indicates gel fraction variation as a function of residence time at various flow rates. It is obvious that the residence time of the rubber in the die is a very important parameter in the devulcanization process. Generally, longer residence time leads to a lower gel fraction. However, as seen from Figure 9(b), this dependence is not unique. It is affected by flow rate. For the same residence time, gel fraction is higher at a higher flow rate.

The fractions of various bonds broken and rates of bond breakup as a function of the distance from the die entrance are presented on Figures 10 and 11. In Figure 11, the normalized rate of bond breakup is defined as $-\{1/[N_i(0)]\}\{[dN_i(t)]/[dt]\}$, where $N_i(t)$ is the number of specific bonds per unit volume at time t, with $N_i(0)$ being the number of bonds per unit volume at initial time $t = 0$. Due to the absence of information concerning the concentration of various crosslinks in the network, the number of monosulfidic and polysulfidic crosslinks is considered to be equal for the present calculations. It is seen from Figure 10 that as the rubber moves away from the horn edge the portion of broken bonds increases monotonically. It is also seen that the number of monosulfidic and polysulfidic bonds bro-

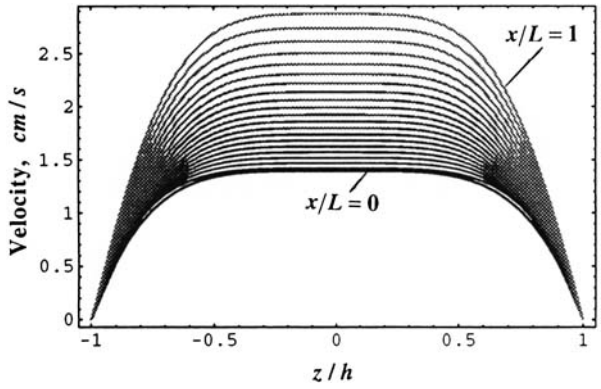

Figure 5 Velocity profiles at various cross sections in the die at flow rate $Q = 0.3$ cm^3/s.

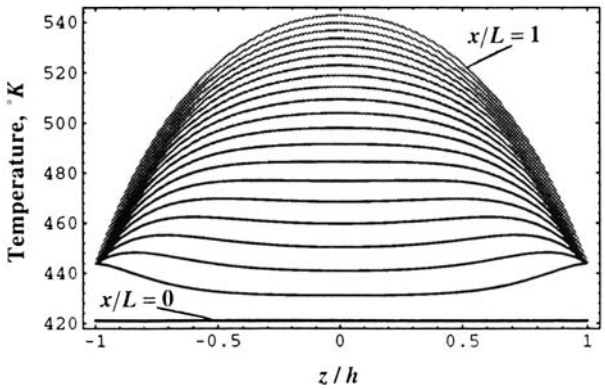

Figure 6 Temperature profiles at various cross sections in the die at flow rate $Q = 0.3$ cm^3/s.

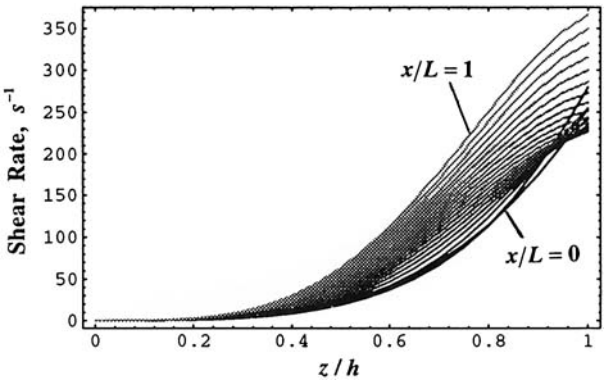

Figure 7 Shear rate profiles at various cross sections in the die at flow rate Q = 0.3 cm^3/s.

ken is always higher then the number of broken carbon–carbon bonds. This observation is consistent with the strength of respective bonds being highest for carbon–carbon and lowest for polysulfidic bonds. It is clear that the ultrasonic devulcanization process does not lead to complete devulcanization, namely, a partial devulcanization takes place accompanied by degradation of the main chain.

From Figure 11, one can observe a maximum in the rate of the breaking of bonds along the die length. The location of this maximum depends on value of the flow rate. At elevated flow rates, the maximum breakup rate is located in the vicinity of the die exit. As the flow rate value reduces, the maximum shifts toward the die entrance until the situation is reached when the rate of bond rupture is highest at die entrance. The bonds are broken up as soon as the vulcanized rubber contacts the edge of the ultrasonic horn. For the lowest flow rate Q = 0.1 cm^3/s, at the die exit about 70% of carbon–carbon, 80% of monosulfidic, and 82% of polysulfidic bonds are broken. The degree of devulcanization is highest for this value of the flow rate. However, it should be noted

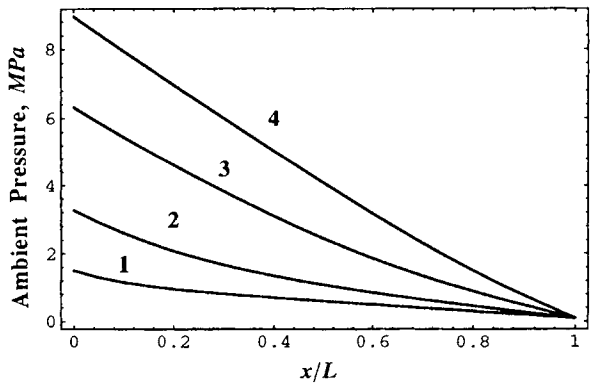

Figure 8 Pressure distribution along die length for various flow rates (cm^3/s): 0.1 (1); 0.2 (2); 0.3 (3); 0.4 (4).

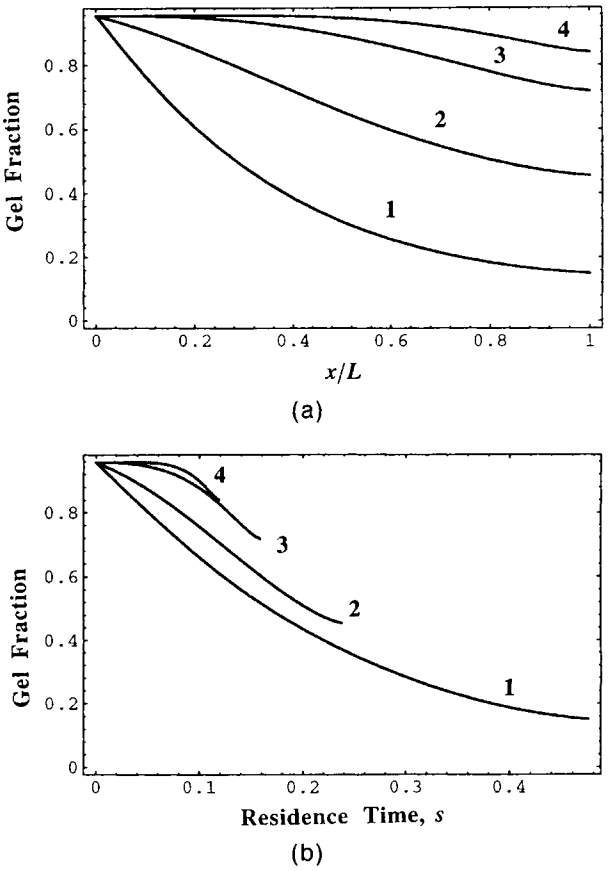

Figure 9 (a) Gel fraction variation along die length and (b) as a function of residence time for various flow rates (cm^3/s): 0.1 (1); 0.2 (2); 0.3 (3); 0.4 (4).

that the lowest flow rate used in experiment is 0.205 cm^3/s. For the highest flow rate, Q = 0.4 cm^3/s, used in the calculations, at the die exit about 9% of carbon–carbon, 12% of monosulfidic, and 12% of polysulfidic bonds are broken.

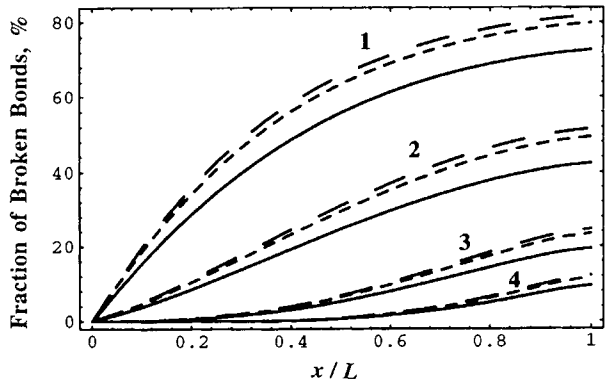

Figure 10 Fraction of various bond ruptures along die length for various flow rates (cm^3/s): 0.1 (1); 0.2 (2); 0.3 (3); 0.4 (4). (Solid line) C—C bonds; (dotted line) C—S—C bonds; (dashed line) C—S_x—C bonds.

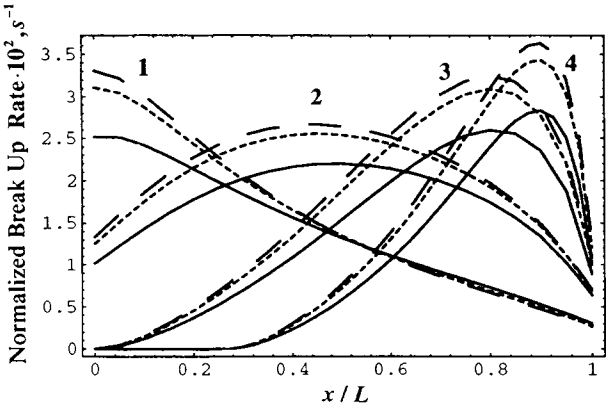

Figure 11 Rate of various bond ruptures along die length for various flow rates (cm^3/s): 0.1 (1); 0.2 (2); 0.3 (3); 0.4 (4). (Solid line) C—C bonds; (dotted line) C—S—C bonds; (dashed line) C—S_x—C bonds.

Now, the questions are: What is the reason for the nonmonotonical behavior of the bond breakup rate, and why is the location of the maximum of this rate along the die length dependent on the flow rate? To answer these questions, one needs to recall the main factors affecting the rate of bond rupture. The rate of bond breakup is determined by (see Part I[1] for details) (1) bond strength, (2) maximum bubble cavitation radius, and (3) concentration of bubbles formed while rubber moves through the die gap. Bond strength is a physical characteristic of a material which is constant. The maximum bubble cavitation radius depends monotonically on ambient pressure. Since the ambient pressure decreases monotonically while rubber flows through the die gap (Fig. 8), the maximum bubble cavitation radius, R_{max}, increases monotonically as the rubber moves toward the die exit. The value of R_{max} as a function of die length depicted in Figure 12 indicates this

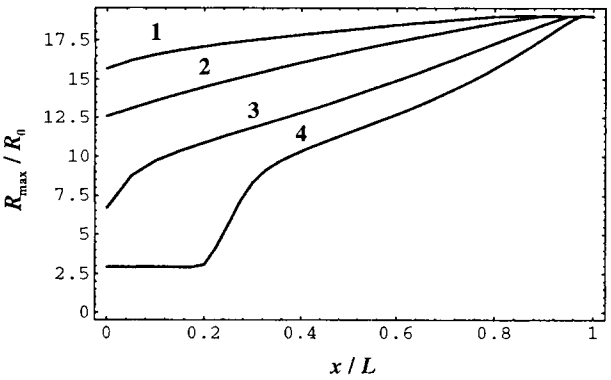

Figure 12 Variation of maximum relative bubble cavitation radius along die length for various flow rates (cm^3/s): 0.1 (1); 0.2 (2); 0.3 (3); 0.4 (4).

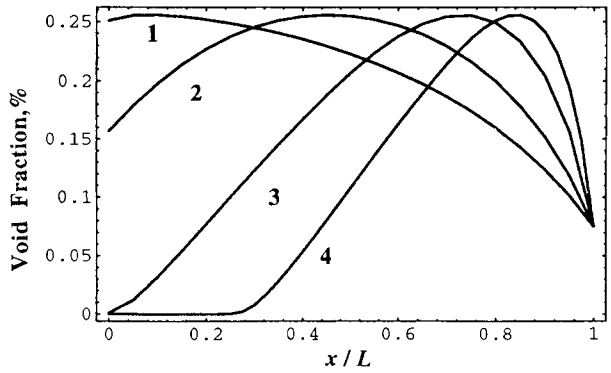

Figure 13 Void fraction variation along die length for various flow rates (cm^3/s): 0.1 (1); 0.2 (2); 0.3 (3); 0.4 (4).

effect. Hence, variation of R_{max} is not responsible for the nonmonotonic behavior of the bond breakup rate. The only remaining reason for the nonmonotonic behavior of the bond breakup rate is the variation of the number of cavitating bubbles along the die length. In Figure 13, the nonmonotonic behavior of the number of primary voids formed is depicted as a function of the die length. Figure 14 is reproduced from Ref. 1 and shows the dependence of the void fraction, φ, on the ambient pressure, P_0. As shown in this plot, the void fraction reaches its maximum value at ambient pressure around 1.2 MPa. Keeping this in mind and referring to Figure 8, one can conclude that the location of the maximum breakup of bonds along the die length roughly corresponds to the distance from the die entrance where the ambient pressure drops down to the value ~ 1.2 MPa. In such a way, there is close correlation between locations of maxima of void fraction and bond breakup rate. However, comparison of Figures 11 and 13 indicate that the location of the maximum bond breakup rate is shifted further downstream with respect to the maximum of the void fraction.

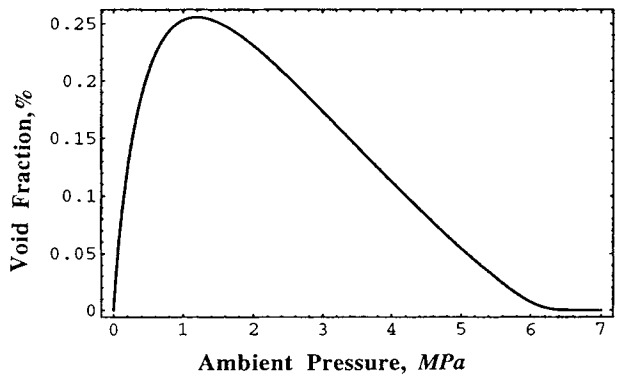

Figure 14 Void fraction as a function of ambient pressure.

This shift is attributed to the fact that the bond breakup rate is proportional to the product of void fraction and bubble cavitation maximum radius, R_{max}. The increase in R_{max} when one moves toward the die exit results in the above-outlined shift of the maxima.

Figure 15 shows the acoustic pressure amplitude variation along the die length. With increasing distance from die entrance, acoustic pressure amplitude decreases due to the decrease in ambient pressure. In addition, an increase in acoustic pressure amplitude with an increase in flow rate is the result of an ambient pressure increase at higher flow rate. The curve 4 in Figure 15 shows that at a high flow rate acoustic pressure amplitude is constant in the region not far from the die entrance. This is due to the fact that in this region ambient pressure is high enough to suppress almost completely the bubble formation and, consequently, acoustic pressure amplitude approaches its upper limit defined by sound velocity in pure rubber (without bubbles).

Figure 16 shows the energy consumed due to devulcanization in absolute units and as a fraction of consumed ultrasound energy which is expended on the heating up of rubber. It is seen that energy consumption due to devulcanization does not exceed 13% of consumed ultrasonic energy. The simulation results show that devulcanization is a complex process involving interaction and mutual influence of different phenomena, such as molecular breakup, material acoustic response, and material rheological and elastic behavior.

Comparison of the Theory with Experiment

In this section, a comparison of the predicted results with experimental data on gel fraction, crosslink density, temperature, and pressure reported in Ref. 2 is made. The predicted and experimental results for gel fraction are presented in Figure 17 for various conditions of devulcanization. Comparison indicates that the theory is qualitatively correct in capturing a tendency of gel fraction variation of devulcanized rubbers with increasing flow rate. However, the theory shows a stronger effect of flow rate and ultrasonic amplitude on gel fraction than the experiment has indicated.

Figure 18 shows a comparison of the predicted and experimental data for crosslink density of devulcanized rubber as a function of flow rate. The predicted crosslink density increases as flow rate increases. This is in contrast to experimental data which show the opposite trend. It should be noted that in carrying out these experiments the horn and die were not cooled. The latter may lead to overheating of the rubber, leading to excessive thermal degradation of rubber which is not taken into account in the present simulation. The above-men-

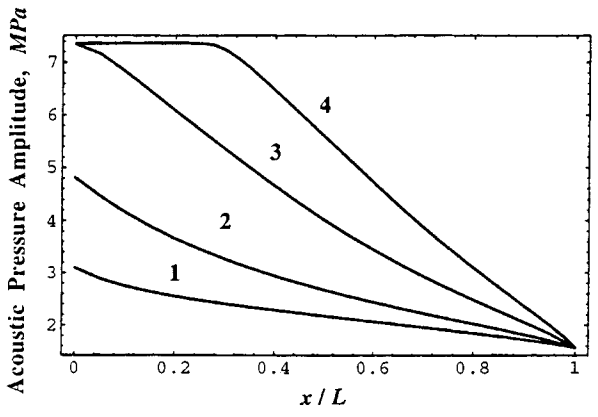

Figure 15 Acoustic pressure amplitude variation along die length for various flow rates (cm^3/s): 0.1 (1); 0.2 (2); 0.3 (3); 0.4 (4).

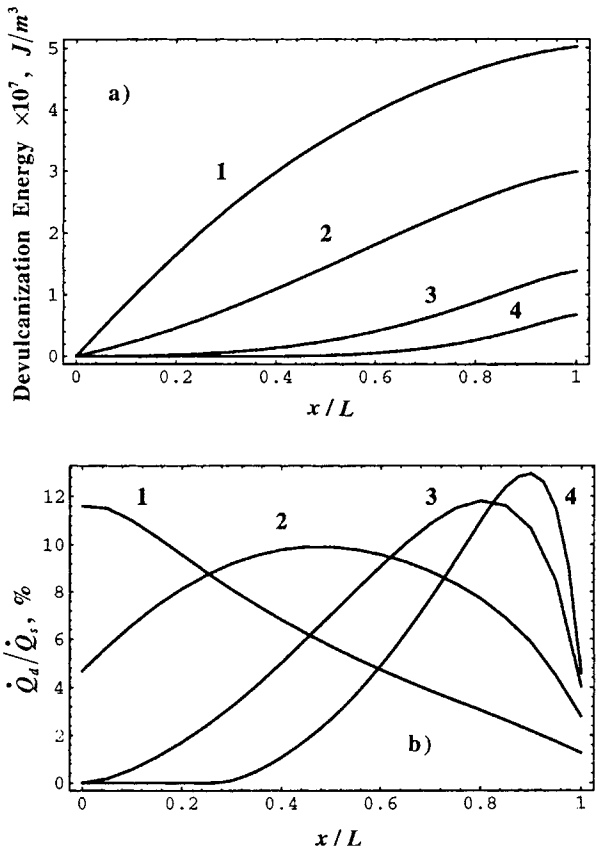

Figure 16 (a) Variation of devulcanization energy consumption and (b) ratio of devulcanization energy consumption to energy expended on ultrasonic dissipation along die length for various flow rates (cm^3/s): 0.1 (1); 0.2 (2); 0.3 (3); 0.4 (4).

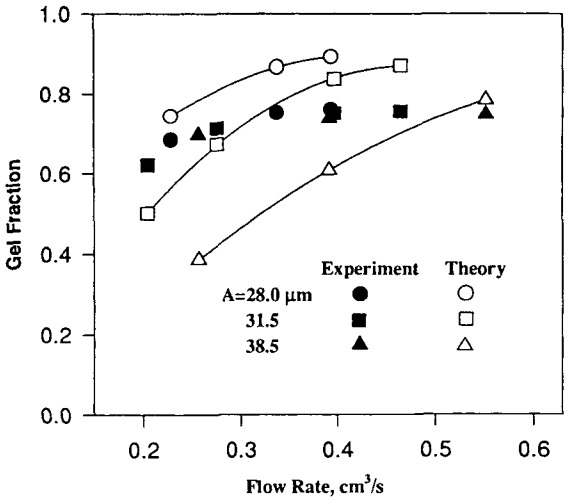

Figure 17 Theoretical (lines with open symbols) and experimental (closed symbols) gel fraction of the devulcanized SBR vs. flow rate.

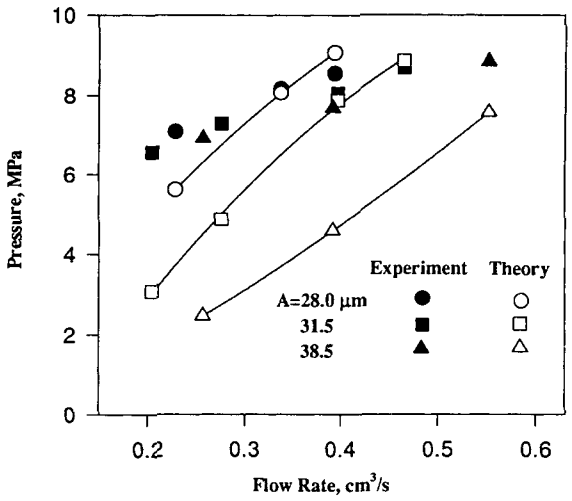

Figure 19 Theoretical (lines with open symbols) and experimental (closed symbols) pressure vs. flow rate.

tioned reasoning may be a plausible explanation for the qualitatively opposite trend observed in the theoretical and experimental behavior of crosslink density of devulcanized rubber as a function of flow rate.

Figure 19 shows the predicted and experimental die characteristics in the devulcanization process. In general, the predicted pressures are lower than the experimental ones. This discrepancy is because the pressure transducer is located at some distance from the die entrance (see Fig. 1), leading to an extra pressure drop. Moreover, an extra pressure drop arises due to the entry and exit pressure losses which are not taken into account in the present simulation. It should be also noted that the theory shows a stronger effect of flow rate and amplitude on pressure than the experiments indicate.

Predicted and experimental temperature dependencies on the flow rate are shown in Figure 20. Predicted temperatures are calculated at the die exit as "mixing cup temperatures," i.e., velocity weighted-average temperatures. It can be seen that the predicted temperatures are very sensitive to ultrasonic amplitude and flow rate variation, namely, as the amplitude increases, the temperature also increases due to higher dissipation of the ultrasonic energy. On the other hand, as the flow rate increases,

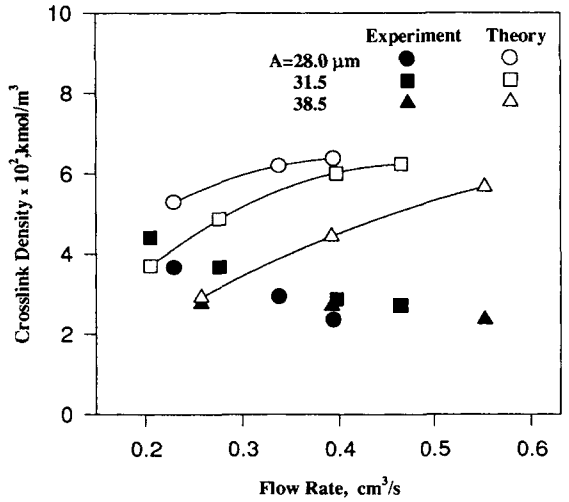

Figure 18 Theoretical (lines with open symbols) and experimental (closed symbols) crosslink density of the devulcanized SBR vs. flow rate.

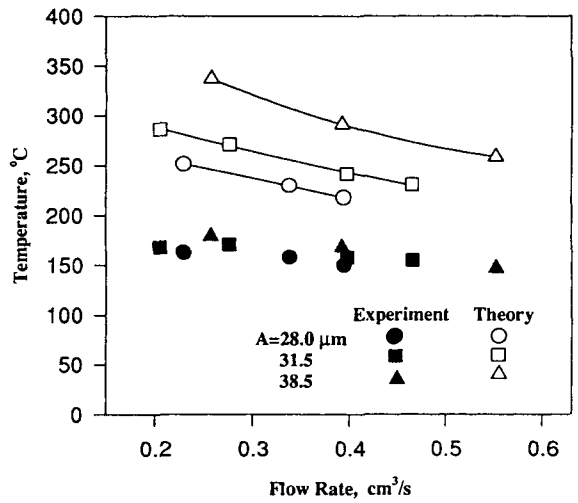

Figure 20 Theoretical "mixing cup temperatures" (lines with open symbols) at the die exit and experimental temperature (closed symbols) as a function of flow rate.

the temperature decreases due to the decrease of the residence time of the rubber in the die. Qualitatively, a similar tendency is observed in the measured temperatures. However, the measured temperatures are significantly lower than are the predicted ones. The highest difference between experimental and calculated temperatures is about 150°C and is observed at the lowest flow rate and highest amplitude. This difference is due to the difficulties in temperature measurements. The thermocouple is placed in the bottom plate of the die where temperature gradients caused by conduction could be quite substantial.

CONCLUSIONS

The present study describes the simulation and experimental results related to a novel ultrasonic devulcanization technology for recycling used tires and other rubber waste. A model of the devulcanization based on the presence of cavitation in rubber vulcanizates proposed in Ref. 1 is utilized to simulate the process. Some experimental evidence is given indicating the presence of cavitation in the devulcanization process. Velocity, temperature, pressure fields, and structural characteristics such as gel fraction and fraction of broken bonds are calculated. The predicted results are found to be in qualitative agreement with experimental data. Theoretical and experimental data indicate that ultrasonic devulcanization leads to a partial devulcanization along with main chain degradation. Future efforts should be directed toward improvement of the proposed model and accumulation of more experimental data related to physical and structural properties of devulcanized rubber. New experimental data should be obtained in the ultrasonic reactor where a special arrangement is made for removal of heat generated due to dissipation of ultrasonic energy.

This work was supported by Grant DMI-9312249 from the National Science Foundation, Division of Engineering.

REFERENCES

1. A. I. Isayev, S. P. Yushanov, and J. Chen, to appear.
2. A. I. Isayev, J. Chen, and A. Tukachinsky, *Rubb. Chem. Technol.*, **68**, 267 (1995).
3. P. J. Flory, *J. Chem. Phys.*, **18**, 108 (1950).
4. K. S. Suslik, *Ultrasound: Its Chemical, Physical, and Biological Effects*, VCH, New York, 1988.
5. S. L. Peshkovskii, M. L. Friedman, A. I. Tukachinskii, G. V. Vinogradov, and N. S. Enikolopian, *Polym. Compos.*, **4**, 126 (1983).
6. A. I. Isayev, *Proceedings of the 23rd Israel Conference on Mechanical Engineering*, Haifa, 1990, Paper #5.2.3.
7. A. I. Isayev and S. Mandelbaum, *Polym. Eng. Sci.*, **3**, 1051 (1991).
8. M. M. Cross, *Rheol. Acta*, **18**, 609 (1979).
9. W. J. Roff and J. R. Scott, *Handbook of Common Polymers*, Butterworth, London, 1971.
10. F. R. Young, *Cavitation*, McGraw-Hill, London, 1989.
11. K. Kircher, *Chemical Reactions in Plastics Processing*, Hanser, New York, 1987.
12. J. R. Woltre, Jr., T. L. Paugh, and A. S. Killian, *Rubb. Chem. Tech.*, **41**, 1329 (1968).
13. A. N. Gent and A. G. Thomas, *J. Polym. Sci.*, **28**, 623 (1958).

Received June 16, 1995
Accepted August 11, 1995